Journal of the European Ceramic Society **18** (1998) 1857–1867

PII: S0955-2219(98)00125-3
0955-2219/98/$—see front matter

Ultrasonic Investigation of the Time-dependent Damage in a 2D SiC/SiC Composite Under Static Loading

J. Chevalier,* M. Huger, D. Fargeot and C. Gault

Laboratoire Matériaux Céramiques et Traitements de Surface, ENSCI, 47 Avenue A. Thomas, 87065 Limoges, France

Abstract

A time dependence of damage under static tensile loading is observed at room temperature in a 2D SiC/C/SiC composite by means of ultrasonic measurements of uniaxial Young's modulus, associated with acoustic emission and strain measurements. During ageing under a constant stress above the threshold level necessary for the first crack initiation in the matrix, a significant decrease of Young's modulus with time occurs, correlated with acoustic emission, which indicates a damage evolution. Additionally it is found that both elastic and inelastic strains increase with time. These static fatigue effects depend on the loading conditions (loading rate and maximum stress level) and lead either to an equilibrium state or to delayed failure for sufficiently high stresses. An interfacial shear stress dependence upon the load level is the most probable mechanism to explain these phenomena. © *1998 Elsevier Science Limited. All rights reserved*

1 Introduction

Long fibre ceramic matrix composites (CMCs) exhibit a non-linear tensile stress–strain behaviour when the stress becomes superior to a threshold value σ_{mc} corresponding to the first microcracking in the matrix. This mechanism strongly depends on the fibre-matrix interface mechanical properties, namely debonding energy and interfacial shear stress τ; it has been extensively investigated by monotonic loading experiments at room temperature. Moreover, numerous modelling approaches have been developed for relating damage and macromechanical parameters (stiffness, elastic and inelastic strains, permanent deformation when unloading) to the constitutive parameters.[1–8] Thus damage processes in CMCs during monotonic loading–unloading sequences, considered as quasi-static solicitations are now rather well understood.

Recently, fatigue of CMCs has received a great deal of attention, and a lot of work on cyclic fatigue has been published.[9–12] Some authors have also reported a degradation of CMCs under static loading,[13–15], but static fatigue and, more generally, time-dependent behaviour under constant tensile stress are poorly documented, despite their practical interest for industrial applications. At room temperature, two phenomena have to be considered:

1. subcritical crack growth (SCG) in the constituents (fibre, matrix or interphase);
2. delayed damage which can be correlated to a dependence of the constitutive parameters (in particular of τ) on the loading conditions (stress level and stress rate).

SCG is classically observed at room temperature in glass[16] and in ceramic oxides[17] under water vapour for long time ageing. Significant increases of crack densities accompanied by stiffness decreases under static loading have been found in SiC/glass–ceramic composites by some authors,[13,15,18] which were attributed to stress corrosion in the glass matrix. For non oxide ceramic like SiC, SCG is negligible in air at room temperature.[19] Therefore, for SiC/SiC composites, other mechanisms must be considered to explain such a time-dependent behaviour. Moreover, in SiC/CAS, Sorensen *et al.*[20] found a strong influence of the loading rate on the monotonic tensile stress–strain behaviour and they interpreted these results by assuming that the interfacial shear stress τ might be dependent on the loading rate.

This paper investigates the existence of such mechanisms in SiC/SiC composites. The damage

*To whom correspondence should be addressed at GEMPPM, INSA, 20 Avenue A. Einstein, 69621 Villeurbanne, France. Fax: (33) 4 72 43 85 28.

induced by tensile loading is evaluated by using a specific equipment which simultaneously allows for a given stress σ:

- the ultrasonic measurement of the macroscopic uniaxial Young's modulus E;
- the associated strain ε;
- the acoustic emission activity AE.

Figure 1 shows a typical tensile curve for CMCs with the mechanical parameters of interest. The initial Young modulus E_o which can be obtained, in our case, from ultrasonic velocity measurements before loading, corresponds to the value usually estimated from the slope of the stress–strain curve in the linear domain. In the non linear domain, the measured strain ε, at a given stress σ, is the sum of the elastic strain ε_e of the microcracked composite and of the inelastic strain ε_{in} which is caused by fibre-matrix sliding and residual misfit strain release.[4] Therefore, it is difficult to distinguish, during loading, the elastic part and the inelastic part of the strain from the stress–strain curve. One solution to obtain the elastic contribution at a given stress level σ is to evaluate the Young's modulus E from the slope of the stress–strain curve at the beginning of unloading. At this specific point, it can be assumed that the inelastic part associated with fibre-matrix sliding is negligible. An other solution, which was used in the present work, is to evaluate Young's modulus E by ultrasonic measurements during the tensile test, at each point of the stress–strain curve.

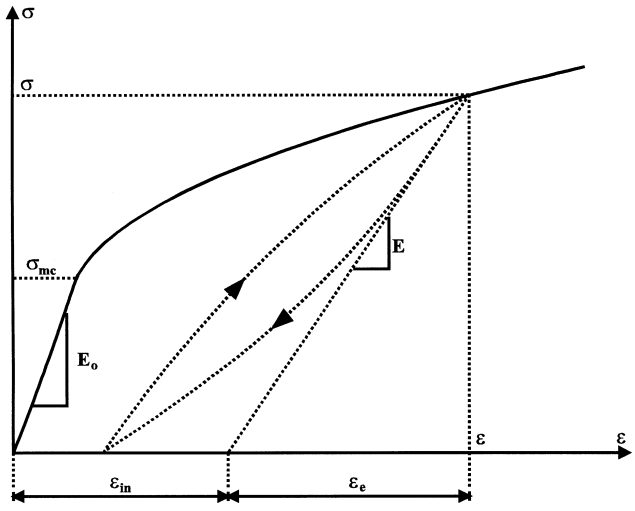

Fig. 1. Typical tensile stress–strain curve of a CMC. The measured parameters at a given σ are E and ε.

Société Européenne de Propulsion, Le Haillan, Saint Médard en Jalles, France.

By measuring E from ultrasonic velocity for a given value of σ, ε_e is obtained by:

$$\varepsilon_e = \sigma/E \tag{1}$$

And ε_{in} is then given by:

$$\varepsilon_{in} = \varepsilon - \sigma/E \tag{2}$$

In the present work, E, ε_e, ε_{in} and AE have been followed during two kinds of experiments:

- monotonic loading at different rates;
- static fatigue tests under various constant stresses.

Using micromechanic models, results are discussed in terms of delayed damage mechanisms induced by variations of the interfacial shear stress τ in longitudinal tows.

2 Experimental

2.1 Material

The material is a 2D SiC/SiC composite made by SEP* by chemical vapour infiltration of a SiC matrix into a preform made by packing 0/90° woven fabrics of Si–C–O Nicalon NLM 202 fibres. The plate processed for this study was 8 mm thick, i.e. thicker than the standard ones fabricated by SEP. The consequence was a higher porosity (~15%), lower mechanical properties (Young's modulus ~180 GPa, tensile strength ~150 MPa) and a density of 2400 kg m^{-3}. A micrograph of the material texture is shown in Fig. 2. As it is usual in this kind of composite,[21] a thin (< 100 nm) carbon interphase ring was observed at high magnification around the fibres. However the composite which have been studied here exhibits a rather limited domain of non linear deformations (typically 0·1 to

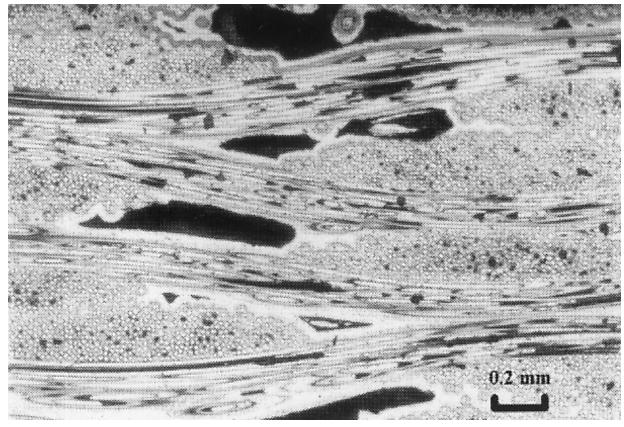

Fig. 2. SEM picture of the texture of the composite.

0·15%). This very low strain–to–failure could be explained by a rather low value of the interfacial shear stress τ which is have been estimated at about 60 MPa[22] in similar 2D SiC/SiC composite.

2.2 Testing apparatus

A schematic diagram of the test fixture is given in Fig. 3(a). The testing device both allows tensile loading and propagation of an ultrasonic longitudinal pulse along the axis of the sample. Details are given elsewhere.[23] The stress in the specimen is calculated from the applied load measured with a load cell attached to the upper ram, with an accuracy of $\pm 2\%$. In order to verify that no noticeable bending occurred in the sample, two electrical strain gauges are attached on both sides of the sample. The strain ε is obtained from the average value of the two gauges results, with an accuracy of $\pm 1\%$.

An alumina waveguide is fixed at the bottom of the sample with an appropriate glue to transmit the ultrasonic pulse emitted by a magnetostrictive transducer. Propagation takes place in the long bar mode and a pattern of successive echoes corresponding to round trips in the sample is obtained. The geometry of the dog bone shaped samples has been optimized with respect to propagation conditions by using a mathematical model,[24] which was used also to calculate the effective sample length, $l_o = 115$ mm. The dimensions of the samples are given in Fig. 3(b). The propagation time t in the sample, corrected from the phase delay in the heads, is obtained by an intercorrelation method from a Fourier analysis of the signal. The ultrasonic velocity V in the long bar mode is then given by:

$$V = 2 \cdot l_o / t \tag{3}$$

And the uniaxial Young modulus E is obtained by:

$$E = \rho \cdot V^2 \tag{4}$$

where ρ is the density of the composite.

Additional AE records were performed during the tests. A computerized AE system (LOCAN 320) was used to plot cumulative AE and AE amplitude distribution versus the stress–strain curves.

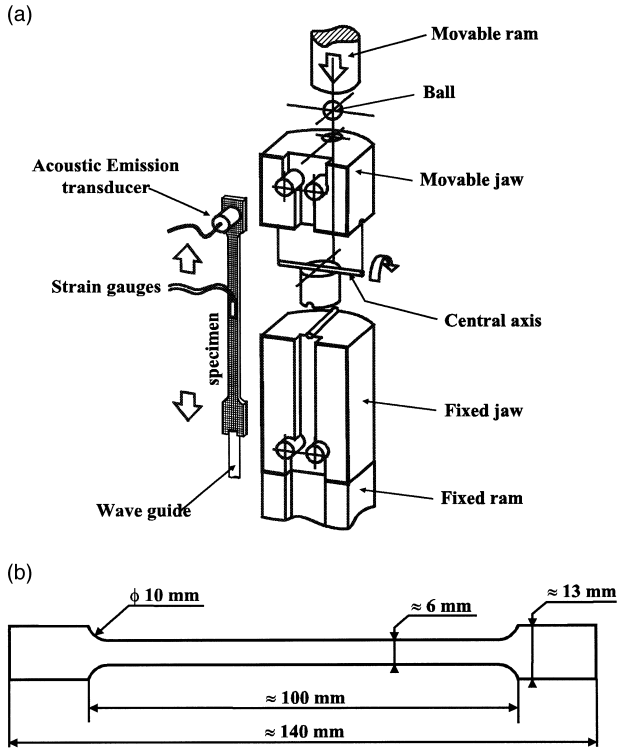

Fig. 3. (a) System for ultrasonic measurement of Young's modulus under tensile loading. (b) Geometry of the dog-bone sample.

3 Results

3.1 Monotonic loading characteristics

The stress–strain curve with the associated cumulative AE data obtained during a monotonic tensile test performed at a stressing rate of 0·3 MPa s^{-1} are reported in Fig. 4. Fig. 5 shows the ultrasonic measurement of E plotted versus the increasing stress. Four damage stages can be distinguished:

- Stage I ($0 < \sigma < 60$ MPa):
  The σ–ε curve is linear and reversible and no AE is detected. The behaviour of the material is elastic-linear. For $\sigma = 0$ the ultrasonic measurement of uniaxial Young's modulus gives the same value, $E_0 = 180$ MPa, as the slope at the origin of the σ–ε curve. A slight increase of Young's modulus is observed in stage I, which is probably due to a stiffening effect due to a trend to decrease of the waviness when the composite is loaded.[25] Nevertheless it can be considered as constant within the experimental error.
- Stage II ($60 < \sigma < 70$ MPa):
  The σ–ε curve remains linear, which is confirmed by the stability of E in Fig. 5, but some AE events are detected above $\sigma_{mc} = 60$ MPa, which are indicators of the formation of the first microcracks in the matrix[26] that probably initiated at the intertow macropores.[8] At this early microcracking stage, the density of microcracks is not large enough to affect the macroscopic stiffness of the composite.

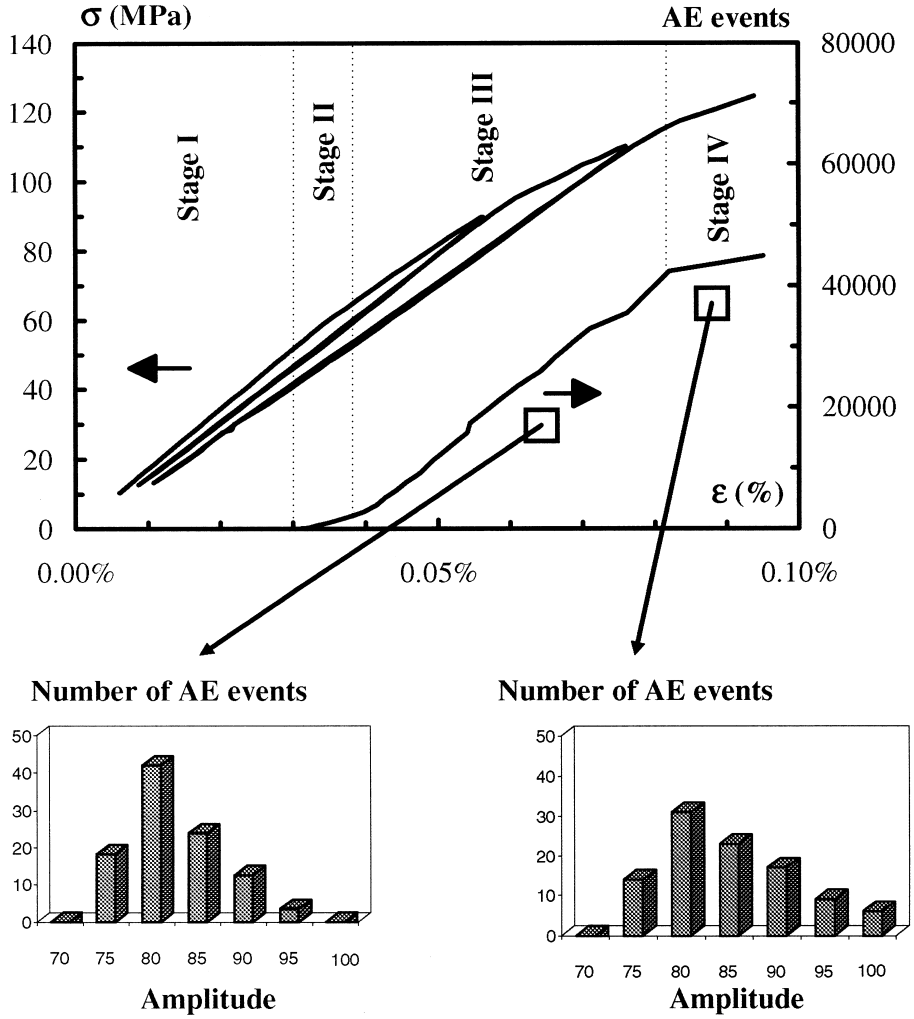

Fig. 4. Tensile stress–strain curve obtained during monotonic loading at 0·3 MPa s^{-1} and two unloading–loading cycles at 90 and 110 MPa, with the associated cumulative *AE* curve and amplitude distribution diagrams in stages III and IV.

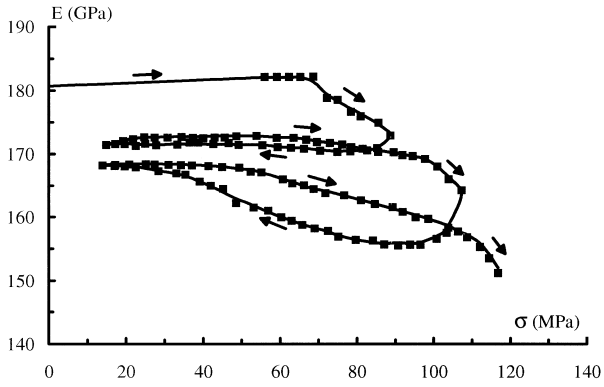

Fig. 5. Variation of Young's modulus *E* versus tensile stress as measured by the ultrasonic method during the test of Fig. 4.

- Stage III ($70 < \sigma < 120$ MPa):

  $\sigma_e = 70$ MPa is the so-called elastic limit which corresponds to the apparent end of the linear portion of the σ–ε curve. Above this value, the *AE* activity steadily increases with the same rate up to 120 MPa and the σ–ε curve becomes non linear. At this stage most of the microcracks have been initiated at the intertow macropores and some of them can cross longitudinal tows. Therefore, subsequent transverse matrix cracking and fibre/matrix debonding begin to occur in longitudinal tows at this stage. It is confirmed by the decrease of *E* associated to the density of opened cracks for $\sigma > 70$ MPa in Fig. 5.

- Stage IV ($\sigma > 120$ MPa):

  A change of damaging regime occurs which is characterized by a lower rate of *AE*. Additionally, Fig. 4 shows that the amplitude distribution of *AE* in stage IV is shifted towards high amplitudes compared to AE in stage III. It has been shown that high amplitude *AE* is associated to fibre breaking, though lower amplitudes are associated to matrix cracking and interfacial debonding.[26] Therefore, $\sigma_s = 120$ MPa is considered to be the saturation limit where a maximum is reached for matrix crack density, where stress in the matrix no more increases and where stresses in the fibres increase quasi-linearly.[3–5] Failure occurs statistically when the remaining

undamaged fibres are stressed above their strength.

3.2 Effect of loading rate on stress–strain curves

Monotonic tensile tests were performed at two different loading rates: $0{\cdot}9\,\mathrm{MPa\,s^{-1}}$ and $0{\cdot}009\,\mathrm{MPa\,s^{-1}}$. The resulting σ–ε curves are reported in Fig. 6(a) and the associated variations of E versus σ are given in Fig. 6(b).

The results show that both σ_e and the strain for a given stress level are affected by the loading rate: for $\sigma = 120\,\mathrm{MPa}$, ε is 25% higher and E is 5% lower at $0{\cdot}009\,\mathrm{MPa\,s^{-1}}$ than at $0{\cdot}9\,\mathrm{MPa\,s^{-1}}$. This suggests that the damage state in the composite under a given level of stress increases when the loading rate decreases and that a steady state of damage can be only achieved for very low loading rates. As mentioned in the introduction, this delayed damage mechanism is a source of static fatigue. Therefore experiments under constant loading were performed.

3.3 Behaviour under constant loading

E, ε and AE were followed versus time after loading at $0{\cdot}3\,\mathrm{MPa\,s^{-1}}$ up to a constant stress σ_c. Four values of σ_c were chosen in relation with the different stages determined on the σ–ε curve of Fig. 4:

- $\sigma_{c1} = 40\,\mathrm{MPa}$ is situated under σ_{mc}, i.e. in the supposed elastic-linear domain;
- $\sigma_{c2} = 60\,\mathrm{MPa}$ corresponds to the first crack initiation;
- $\sigma_{c3} = 90\,\mathrm{MPa}$ is in the non linear domain (stage III), where matrix microcracking and fibre/matrix debonding are predominant;
- $\sigma_{c4} = 120\,\mathrm{MPa}$ corresponds to σ_s i.e. to crack saturation and to the beginning of stage IV where fibre breaking is statistically expected.

At 40 MPa there were no variations of E and ε and no acoustic event was detected up to 70 h. This confirms that no damage occurs in the elastic-linear stage.

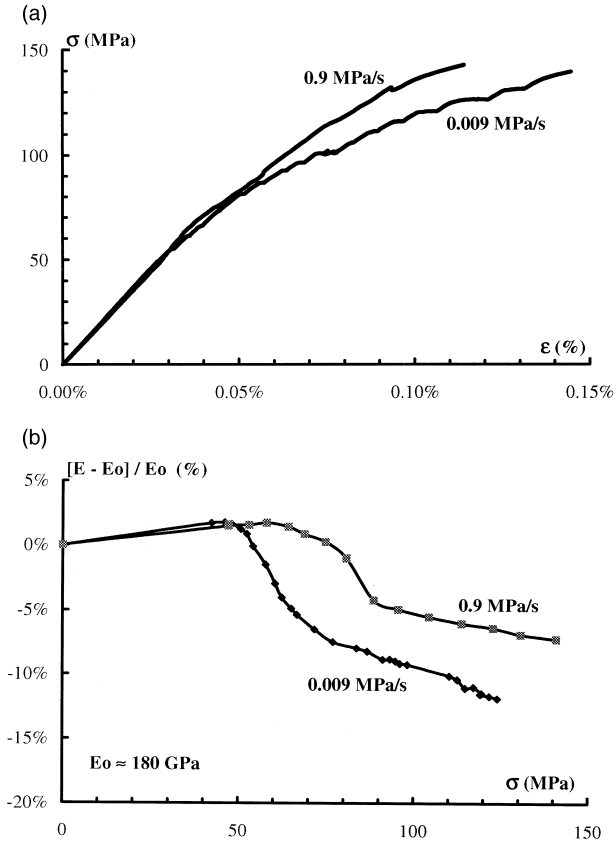

Fig. 6. (a) Tensile stress–strain curves obtained at two different loading rates $0{\cdot}9\,\mathrm{MPa\,s^{-1}}$ and $0{\cdot}009\,\mathrm{MPa\,s^{-1}}$. (b) Associated variations of Young's modulus.

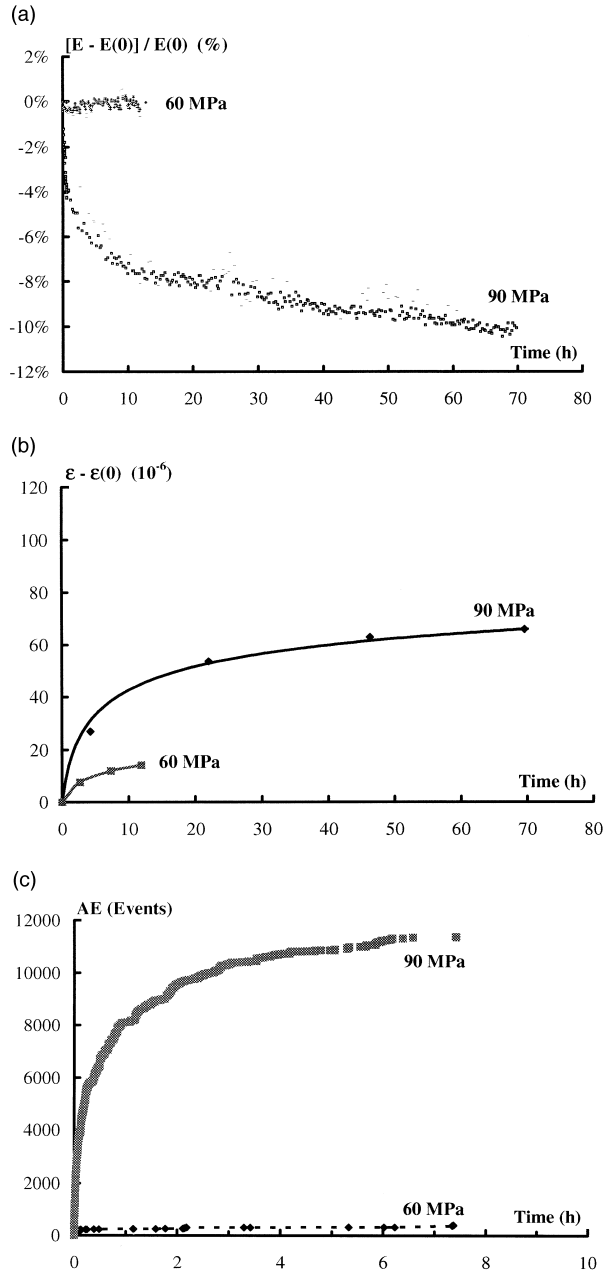

Fig. 7. (a) Relative variations of Young's modulus [$E(0)$ is the value at $t = 0$] versus time under constant tensile stresses 60 and 90 MPa. (b) Strain increase during the same test. (c) Cumulative AE during the first hours of the tests.

Figure 7 gives the results obtained at σ_{c2} and σ_{c3}. At 60 MPa there was no significant variation of E up to 12 h, but the measured strain slightly increased and few AE events were detected during the first minutes of the stress plateau. The test was stopped after 12 h, because no more evolution was observed. These results show that only a small damage occurs at 60 MPa which corresponds to σ_{mc}.

Under 90 MPa, a significant decrease of E, correlated with an increase of ε and a large number of AE events, indicate a damage extension with time. Nevertheless most of the damage occurs during the first hours of the test and both E and ε remain constant after 40 h. This suggests a delayed damage mechanism with a steady state. Furthermore, the AE amplitude distribution was found to be constant and similar to that observed in stage III of the monotonic tensile test (Fig. 4), which proves that the damage modes are similar: matrix microcracking and/or fibre/matrix debonding.

Most of the specimens loaded under 120 MPa failed in the first hours of the test. Deep AE increments and a strong increase of ε were observed before delayed failure. As for stage IV of monotonic loading, the amplitude distribution of the AE events was shifted towards the high values denoting fibre breaking. These results show that rupture by static fatigue may occur in stage IV; further work has to be performed to study this mechanism of failure. Therefore the following discussion only concerns delayed damage which occurs at lower loads.

4 Delayed damage analysis

Experimental results show the existence of a time-dependent damage mechanism when tensile tests under a constant load are performed in stage III, i.e. between σ_{mc} and σ_s (for example under 90 MPa in Fig. 7). This mechanism which leads to a stable damage state is discussed in the following part.

4.1 Elastic and inelastic strains variations associated to delayed damage

The simultaneous measurement of E (equivalent to unloading modulus defined in Fig. 1) and of ε allows the determination of the elastic part ε_e and of the inelastic part ε_{in} of the strain by the way of eqns (1) and (2). They were calculated and plotted versus time for the test under 90 MPa in Fig. 8.

Both ε_e and ε_{in} increase with time before reaching a steady state after 50 h. At the beginning of the test, the inelastic strain, $\varepsilon_{in}(0) \approx 10 \times 10^{-6}$, is low compared to the measured one, $\varepsilon(0) = 520 \times 10^{-6}$ and the origin of strain is mainly elastic. But, though $\varepsilon(t)$ approximately increases of 10% after 50 h, ε_{in} increases of more than 100%. Therefore a static fatigue mechanism at interfaces controlled by delayed debonding may be considered. This should be linked to stress concentration on the interface asperities.[27]

As it has been previously noticed, different sequences of damage development are usually considered in a 2D woven composite subjected to tensile loading.[6–8] Matrix microcracking first starts at the edge of the inter-tows macropores (cf. Figure 2); then some of those microcracks can be deflected at the 90°-tow periphery and the others can cross the 0°-tows before reaching another macropore. For upper load, new microcracks can start at the edge of micropores in a 90°-tow and then propagate through 0°-tows. When microcracks cross 0°-tows, fibre/matrix debonding occurs.

Therefore, for 2D CMCs, it is usual to consider three main sequences of damage:

- inter-tows matrix cracking;
- intra-90°-tows matrix cracking;
- intra-0°-tows matrix cracking with extensive fibre/matrix debonding.

Some of the cracks involved in the two first damage sequences extend towards 0°-tows where they cause transverse cracking with fibre/matrix debonding. Since the composite which has been used for this study, exhibits a rather low strain to failure (typically 0·1% to 0·15%), the third sequence of damage should not occur in our case.

All those kind of damage can affect the macroscopic elastic behaviour (E, ε_e), though the inelastic behaviour (ε_{in}) depends mainly on debonding/sliding mechanisms.

The inelastic strain can be written as the sum of two terms.[4]

$$\varepsilon_{in}(t) = \varepsilon_{in}^{s}(t) + \varepsilon_{in}^{T}(t) \tag{5}$$

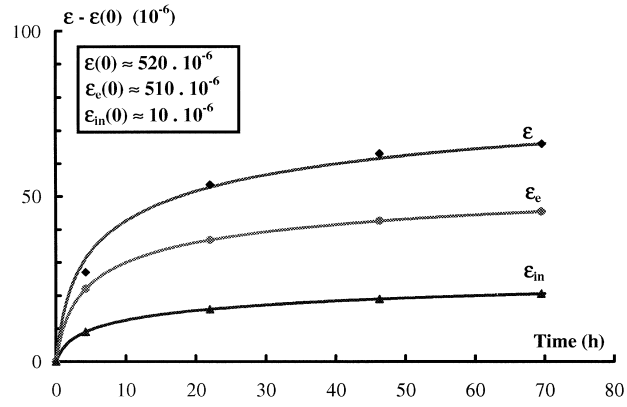

Fig. 8. Increase versus time of the measured strain, ε, of the elastic strain ε_e and of the inelastic strain ε_{in} during the test under 90 MPa.

where $\varepsilon^{s}_{in}(t)$ is the fibre-matrix sliding strain and $\varepsilon^{T}_{in}(t)$ is the residual thermal misfit strain release which is expressed by:[4]

$$\varepsilon^{T}_{in}(t) = q\frac{E_0}{E_m}\left(\frac{1}{E_0} - \frac{1}{E(t)}\right) \quad (6)$$

where E_m is Young's modulus of the matrix and q is the axial residual thermal stress in the matrix.
The consequence is that when $E(t)$ varies under constant load, $\varepsilon^{T}_{in}(t)$ varies too. But a calculation of the order of magnitude of this variation during the test at 90 MPa using eqn (6) and experimental results of Fig. 7(a) gives about -8% which is negligible compared with the amplitude of variation of $\varepsilon_{in}(t)$ ($\approx 100\%$). Consequently fibre-matrix sliding has been considered as the major contribution to the inelastic strain increase under constant load. A possible explanation is an interfacial delayed damage which is expected to be strongly dependent on the morphology of the interfaces.

4.2 Time dependence of the interfacial parameters

Two kinds of approaches may be used for modelling the tensile behaviour of CMCs:

- the first is based on damage mechanics of the composite considered as a continuous medium at mesoscopic and macroscopic scales,[6]
- the second applies micromechanics models to the prediction of the stress–strain curves from constitutive parameters related to the elementary constituents.[3,4]

One advantage of micromechanics models is to lead to equations relating 'elastic' moduli (secant, tangent, or unloading) and the strain (elastic or inelastic) to the interfacial shear stress τ for a given applied tensile stress. But these models have been developed for 1D CMCs and their use for 2D woven composites is not obvious; in particular it is a rather rough approximation in such case to characterize the interfacial sliding mechanisms by a single τ value. Therefore, the following assumptions have been made for interpretation of delayed damage mechanisms:

- the two first damaging sequences, namely inter-tow matrix cracking with some of theses cracks crossing the 0°-tows and intra-90°-tows cracking, occur during loading and remain stable with time under the constant stress;
- the delayed damage mechanism in the 2D composite is governed by damage propagation in the 0°-tows which are considered as 1D composites.

Then a micromechanics model can be used to show whether a time dependence of interfacial properties in the 0°-tows can lead to the delayed damage mechanism observed under constant tensile loading.

Kuo *et al.*[3] have proposed a model with a partial fibre/matrix interfacial debonding for 1D CMC loaded in tension above σ_{mc}. The composite is decomposed into identical unit cells bridged by the fibre. For each cell, the fibre and the matrix are considered as concentric cylinders with radius r_0 and R, respectively; matrix cracks, perpendicular to the fibre, are separated by a distance L and debonding extends on a length L_d around the fibre (Fig. 9). A so-called "shear-lag model" is applied to the bonded region, to calculate the interfacial shear stress which varies along the bonded interface and depends on the stress field in the fibre and in the matrix; the interfacial shear stress is assumed to be a constant τ in the debonded area.

The deformation of the unit cell subjected to a tensile stress σ is given by the following equation:[28]

$$\varepsilon = \frac{\sigma}{E_0^t}\left(1 + 2\cdot a\cdot\frac{L_d}{L}\right) + 2\cdot\frac{\tau\cdot L_d}{E_f\cdot r_0}\cdot\frac{L_d}{L} + \frac{2}{\beta\cdot L}\cdot\tanh[\beta(L/2 - L_d)]\cdot\left(\frac{a\cdot\sigma}{E_0^t} - 2\cdot\frac{\tau\cdot L_d}{E_f\cdot r_0}\right) \quad (7)$$

Where E_f is the fiber Young's modulus along its axis, E_m is the matrix Young's modulus, E_0^t is the Young's modulus of a tow, considered as an ideal 1D composite, without matrix cracking (i.e. before loading), a is the ratio $E_m V_m / E_f V_f$, with V_m and V_f the fractional volume of matrix and fiber in the tow, respectively (cf. Table 1).

β is the shear-lag constant which only depends on the fractional volume and on the mechanical properties of the constituents:[29]

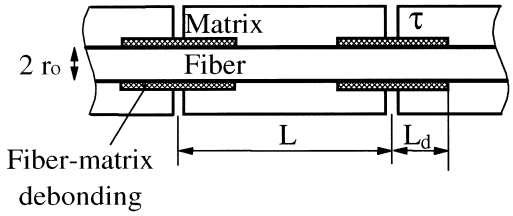

Fig. 9. Unit cell model[3] used for micromechanics analysis in 0°-tows considered as 1D composites.

Table 1. Numerical values of parameters of a 1D SiC/SiC tow

E_m (GPa)	V_m	V_f	E_f (GPa)	r_0 (μm)	E'_0 (GPa)	a
350	0·2	0·6*	200	7	260**	1·17

*Evaluated by SEM observation of a tow cross section.
**Calculated with a mixture law $E_0^t = E_m(1 - V_f) + E_f V_f$.

$$\beta = \left[\frac{2\cdot E_0^t}{E_f\cdot(1-\nu_m)\cdot\left(1n\frac{1}{V_f}+V_f-1\right)}\right]^{1/2}\cdot 1/r_0 \quad (8)$$

with ν_m Poisson's ratio of the matrix.

A numerical calculation of β in the case of a SiC/SiC unidirectional composite, with the values listed in Table 1 shows that the term depending on β in eqn (7) can be neglected. Therefore, eqn (7) can be approximated by:

$$\varepsilon \approx \frac{\sigma}{E_0^t}\left(1+2\cdot a\cdot\frac{L_d}{L}\right)+2\cdot\frac{\tau\cdot L_d}{E_f\cdot r_0}\cdot\frac{L_d}{L} \quad (9)$$

When unloading, L_d/L remains constant and the elastic modulus of the tow, E^t, is obtained by taking the inverse of the derivative of eqn (9) with respect to the applied stress σ as follows:

$$E^t = E_0^t[1+2a\cdot L_d/L]^{-1} \quad (10)$$

By combination with eqn (2), the inelastic strain of the tow is given by:

$$\varepsilon_{in}^t = \frac{2}{E_f\cdot r_0}\cdot\tau\cdot L_d\frac{L_d}{L} \quad (11)$$

Moreover, L_d is a function of τ:

$$L_d = \frac{\sigma\cdot a\cdot r_0}{2V_f(1+a)\tau} \quad (12)$$

Then the inelastic strain of the tow can be written under the form:

$$\varepsilon_{in}^t = A\frac{L_d}{L} \quad (13)$$

with:

$$A = \frac{\sigma\cdot a}{V_f E_f(1+a)} \quad (14)$$

If the tow is subjected to a constant stress σ, A is constant with time and eqn (10) and (13) show that variations of E^t and ε^t_{in} can be provoked by variations of the ratio $x = \frac{L_d}{L}$.

During static fatigue tests, the relative variations versus time of ε^t_{in} and E^t are related to the relative variations of x through eqn (15) and (16) respectively:

$$\frac{\varepsilon_{in}^t(t)-\varepsilon_{in}^t(0)}{\varepsilon_{in}^t(0)} = \frac{x(t)-x(0)}{x(0)} \quad (15)$$

$$\frac{E^t(t)-E^t(0)}{E^t(0)} = -\frac{2a\cdot x(0)}{1+2a\cdot x(0)}\frac{x(t)-x(0)}{x(0)} \quad (16)$$

where $\varepsilon^t_{in}(0)$, $E^t(0)$ and $x(0)$ are the values of inelastic strain, Young's modulus and x ratio under the stress σ at the beginning of the static fatigue test ($t = 0$), respectively.

Therefore by combining eqns (15) and (16):

$$\frac{E^t(t)-E^t(0)}{E^t(0)} = -\frac{2a\cdot x(0)}{1+2a\cdot x(0)}\frac{\varepsilon_{in}^t(t)-\varepsilon_{in}^t(0)}{E_{in}^t(0)} \quad (17)$$

This equation shows that, for static fatigue tests, the relative variations of Young's modulus and of inelastic strain of a tow are proportional.

$\frac{E(t)-E(0)}{E(0)}$ has been plotted versus $\frac{\varepsilon_{in}(t)-\varepsilon_{in}(0)}{\varepsilon_{in}(0)}$ from the experimental results of Fig. 7(a) and Fig. 9 obtained under 90 MPa up to 70 h. The result, given in Fig. 10 shows an approximate linear variation with a slope −0·04.

From this value and within the approximation of delayed damage being controlled by longitudinal tows, an estimation of $x(0)$ can be obtained using eqn (17) with numerical values of Table 1: $x(0) = \frac{L_d}{L}(0) = 0{\cdot}03$. This order of magnitude is consistent with results found for similar SiC/SiC in literature.[30]

By combining of eqns (10), (12), (13), expressions relating E^t and ε^t_{in} to τ are obtained:

$$E^t = E_0^t\left[1+\frac{\sigma a^2 r_0}{V_f(1+a)}\frac{1}{\tau L}\right]^{-1} \quad (18)$$

$$\varepsilon_{in}^t = A^2 r_0 E_f\frac{1}{\tau L} \quad (19)$$

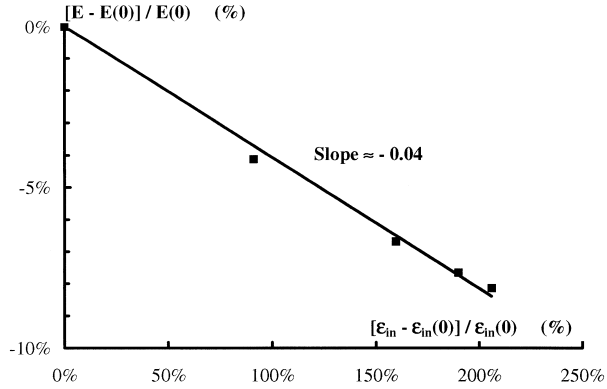

Fig. 10. Relative variations of Young's modulus as a function of relative variations of inelastic strain during the test under 90 MPa.

If debonding extension in the longitudinal tows is assumed to be the dominant mechanism of delayed damage, the crack density L is assumed to be constant under a constant stress level σ. Therefore, an increase of ε^{t}_{in} and a decrease of E^{t} will be caused by a decrease of τ under static loading according to a function τ(t).

Then, with the hypothesis of delayed damage in the 2D composite caused by delayed damage in the 0° tows, the variations of E and ε_{in} for the composite are expected to follow similar variations as given by eqns (20) and (21):

$$E(t) = E_0 \cdot \left(1 + \frac{k_1}{\tau(t)}\right)^{-1} \tag{20}$$

$$\varepsilon_{in}(t) = \frac{k_2}{\tau(t)} \tag{21}$$

where k_1 and k_2 are constants which can be determined from the experimental values $E(0)$ and $\varepsilon_{in}(0)$ at $t = 0$: $k_1 = \frac{\tau(0)[E_0 - E(0)]}{E(0)}$, and $k_2 = \varepsilon_{in}(0) \cdot \tau(0)$.

Introducing a new parameter $\Delta = \frac{E_0 - E(0)}{E(0)}$ which can be experimentally determined after the monotonic loading up to σ, and stating that $\Delta \frac{\tau(0)}{\tau(t)} \ll 1$, eqns (20) and (21) can be rewritten:

$$\varepsilon_{in}(t) = \varepsilon_{in}(0) \frac{\tau(0)}{\tau(t)} \tag{22}$$

$$E(t) = E_0 \cdot \left(1 - \Delta \frac{\tau(0)}{\tau(t)}\right) \tag{23}$$

Then, $\left(\frac{\tau(0)}{\tau(t)} - 1\right)$ is related to the relative variations of E and ε_{in} during the static fatigue test by the two equations:

$$\left(\frac{\tau(0)}{\tau(t)} - 1\right) = \frac{\varepsilon_{in}(t) - \varepsilon_{in}(0)}{\varepsilon_{in}(0)} \tag{24}$$

$$\left(\frac{\tau(0)}{\tau(t)} - 1\right) = \left(\frac{\Delta}{\Delta - 1}\right)^{-1} \frac{E(t) - E(0)}{E(0)} \tag{25}$$

These equations predict, as eqn (17), that $\frac{E(t) - E(0)}{E(0)}$ *and* $\frac{\varepsilon_{in}(t) - \varepsilon_{in}(0)}{\varepsilon_{in}(0)}$ are proportional. The calculation of $\frac{\Delta}{\Delta - 1}$ gives a slope −0·055 which is close to the value (−0·04) found in Fig. 10. The difference comes from the experimental determination of E_0 and $E(0)$ which are real values of Young's modulus of the 2D composite taking into account the texture of the material (in particular porosity) and inter-tows and 90° tows damage. For the following numerical simulation, $\frac{\Delta}{\Delta - 1}$ is taken equal to −0·05.

According to eqn (24) and (25), $\left(\frac{\tau(0)}{\tau(t)} - 1\right)$ can be plotted from the experimental variations of $E(t)$ and $\varepsilon_{in}(t)$ of Figs 7(a) and 8. The result is shown in Fig. 11.

An empirical law has been choosen for $\tau(t)$ in order to obtain the best fit with experimental points:

$$\tau(t) = \tau_{st} + \frac{\tau(0) - \tau_{st}}{(1 + t)^{n}} \tag{26}$$

where τ; (0) is the value of τ at $t = 0$, τ_{st} is the asymptotic value of τ when $t \to \infty$ (i.e. corresponding to steady state) and $n \geq 0$ characterizes the relaxation mechanism of τ under constant tensile loading.

The variations of τ normalised to $\tau(0)$ are then given by:

$$\frac{\tau(t)}{\tau(0)} = \frac{\tau_{st}}{\tau(0)} + \frac{1 - \frac{\tau_{st}}{\tau(0)}}{(1 + t)^{n}} \tag{27}$$

The two parameters $\frac{\tau_{st}}{\tau(0)}$ and n have been adjusted in order to reach the best agreement with experimental data obtained at 90 MPa after loading at 0·3 MPa s^{-1}: Fig. 11 shows the plot of $\left(\frac{\tau(0)}{\tau(t) - 1}\right)$ for $\frac{\tau_{st}}{\tau(0)} = 0{\cdot}3$ and $n = 0{\cdot}8$. Then, in this case, τ was found to decrease of about 70% before reaching equilibrium after 50 h.

These numerical values are depending on the material, in particular on the type of fibre/matrix

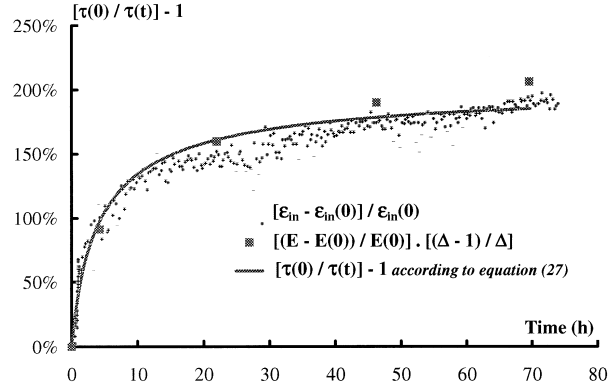

Fig. 11. Comparison between the experimental variation $\left[\frac{\tau(0)}{\tau(t)} - 1\right]$ under 90 MPa obtained from data of variations of $E(t)$ (small points) and of $\varepsilon_{in}(t)$ (dark squares), and the curve calculated with eqn (27) for $\frac{\tau_{st}}{\tau(0)} = 0{\cdot}3$ and $n = 0{\cdot}8$.

interphase, but probably also on the load level and on the initial loading rate. Further work is necessary to determine the relationships between the relaxation of the interfacial shear stress in the longitudinal tows and interface parameters. One hypothesis could be a smoothing of the contact surface between fibre and matrix due to stress concentrations on the asperities when loading.

5 Conclusion

A time dependence of damage monitored by uniaxial Young's modulus and strain measurements has been found at room temperature in SiC/SiC fibrous composites subjected to tensile stress above the threshold matrix microcracking stress. One hypothesis to explain this behaviour is to assume a relaxation of the interfacial shear stress in the longitudinal tows. According this assumption, after loading the material up to 90 MPa at 0·3 MPa s^{-1}, τ was found to decrease of about 70% before reaching equilibrium after 50 h. One consequence of this mechanism is a dependence on loading rate of the experimental monotonic tensile stress-strain curves obtained from monotonic tensile tests in CMCs: testing under true static loading conditions requires very low stressing rates.

Acknowledgements

The authors would like to thank the S.E.P. Society (St Médard en Jalles, France) for processing the composites and Dr P. Reynaud from G.E.M.P.P.M. (I.N.S.A. Lyon, France) for helpful discussion.

References

1. Aveston, J., Cooper, G. A. and Kelly, A., Single and multiple fracture. In *The Properties of Fiber Composites*. Proc. of Nat. Phys. Lab. Conf., Guilford, UK. IPC Sci. & Tech. Press, Teddington, UK., 1971, pp. 15–26.
2. Evans, A. G. and Marshall, D. B., The mechanical behavior of ceramic matrix composites. *Acta Metall. Mater.*, 1989, **37**, 2567–2583.
3. Kuo, W. S. and Chou, T. W., Multiple cracking of unidirectional and cross-ply ceramic matrix composites. *J. Amer. Ceram. Soc.*, 1995, **78**(3), 745–755.
4. Vagaggini, E., Domergue, J. M. and Evans, A. G., Relationships between hysteresis measurements and the constituent properties of ceramic matrix composites: I, Theory. *Amer. Ceram. Soc.*, 1995, **78**(10), 2709–2720.
5. Domergue, J. M., Vagaggini, E. and Evans, A. G., Relationships between hysteresis measurements and the constituent properties of ceramic matrix composites: II, Experimental studies on unidirectional materials. *J. Amer. Ceram. Soc.*, 1995, **78**(10), 2721–2731.
6. Aubard, X., Lamon, J. and Allix, O., Model of the non linear mechanical behavior of 2D SiC/SiC chemical vapor infiltration composites. *Amer. Ceram. Soc.*, 1994, **77**(8), 2118–2126.
7. Guillaumat, L., Microfissuration des CMC: Relation avec la microstructure et le comportement mécanique. Ph.D. Thesis, Bordeaux I University, France, 1994.
8. Guillaumat, L. and Lamon, J., Multi-fissuration de composites SiC/SiC, Revue des composites et matériaux avancés, Editions Hermès, Paris, 1993, pp. 159–171.
9. Kotil, T., Holmes, J. W. and Comninou, T., Origin of hysteresis observed during fatigue of ceramic matrix composites. *J. Amer. Ceram. Soc.*, 1990, **73**(7), 1879–1883.
10. Zawada, L. P., Buktus, L. M. and Hartman, G. A., Tensile and fatigue behavior of silicon carbide fiber reinforced aluminosilicate glass. *Amer. Ceram. Soc.*, 1991, **74**(11), 2851–2858.
11. Reynaud, P., Rouby, D. and Fantozzi, G., Effects of interfacial evolutions on the mechanical behavior of ceramic matrix composites during cyclic fatigue. *Scripta Metall. Mater.*, 1994, **31**(8), 1061–1066.
12. Evans, A. G., Zok, F. W. and McMeeking, R. M., Fatigue of ceramic matrix composites. *Acta Metall. Mater.*, 1995, **43**, 859–875 .
13. Karandikar, P. G. and Chou, T. W., Damage development and moduli reductions in Nicalon–calcium aluminosilicate composites under static fatigue and cyclic fatigue. *Amer. Ceram. Soc.*, 1993, **76**(7), 1720–1728.
14. Despierres, T., Etude de l'endommagement des SiC/SiC faible et forte déformations sous sollicitation quasi-statique et en fatigue. Ph.D. Thesis, Caen University, France, 1994.
15. Gomina, M., Quasi-static and fatigue damage accumulation in a Nicalon–lithium magnesium aluminosilicate composite material. In *High-Temperature Ceramic-Matrix Composites 1*, ed. A. G. Evans, and R. Naslain, *Ceram. Trans.*, 1995, **57**, 335–342.
16. Wiederhorn, S. M., Influence of water vapour on crack propagation in soda-lime glass. *Amer. Ceram. Soc.*, 1967, **50**, 407–414.
17. Chevalier, J., Etude de la propagation des fissures dans une zircone 3Y-TZP pour applications biomèdicales. Ph.D. Thesis, INSA Lyon, France, 1996.
18. Spearing, S. M., Zok, F. W. and Evans, A. G., Stress coorsion cracking in a unidirectional ceramic-matrix composite. *J. Amer. Ceram. Soc.*, 1994, **77**(2), 562–570.
19. Ohji, T., Yamauchi, Y., Kanematsu, W. and Ito, S., Dynamic and static fatigue strength and crack propagation of engineering ceramics. *J. Japan Ceram. Soc.*, 1990, **98**(6), 521–528.
20. Sorensen, B. F. and Holmes, J. W., Effect of loading rate on the monotonic tensile behavior of a continuous-fiber-reinforced glass–ceramic matrix composite. *J. Amer. Ceram. Soc.*, 1996, **79**(2), 313–320.
21. Huger, M., Fargeot, D. and Gault, C., Ultrasonic characterization of oxidation mechanisms in Nicalon/C/SiC composites. *J. Amer. Ceram. Soc.*, 1994, **77**(10), 2554–2560.
22. Passilly, B., Sudre, O. and Parlier, M., Caractérisation mécanique des interfaces dans les composites céramique–céramique. In *Revue des composites et matériaux avancés*. Editions Hermès, Paris, 1993, pp. 253–265.
23. Cutard, T., Huger, M., Fargeot, D. and Gault, C., Ultrasonic characterization at high temperature of damage in ceramic composites subjected to tensile stresses. In *High Temperature Ceramic Matrix Composites*, ed. R. Naslain, J. Lamon and D. Doumeingts, Woodhead Publishing, Cambridge, UK, 1993, pp. 699–706.
24. Cutard, T., Fargeot, D., Gault, C. and Huger, M., Ultrasonic measurements of Young's modulus in 'dog bone' shape samples subjected to tensile stress. *J. Appl. Phys.*, 1994, **76**(1), 126–132 .
25. Hsiao, H. M. and Daniel, I. M., Elastic properties of composites with fiber waviness.. *Composites Part A*, 1996, **27A**, 931–941.

26. Tsuda, H., Takahashi, J., Kemmochi, K. and Hayashi, R., Fracture process of silicon carbide fiber-reinforced glasses. *J. Amer. Ceram. Soc.*, 1996, **79**(9), 2293–2299.
27. Cherouali, H., Reynaud, P. and Rouby, D., Phénomènes de frottement lors du glissement interfacial dans les composites modèles monofilamentaires à matrice fragile. *Revue des composites et matériaux avancés*. Editions Hermès, Paris, 1997, pp. 139–167.
28. Kuo, W. S. and Chou, T. W., Modelling of the thermomechanical behavior of glass matrix composites. In *Metal and Ceramic Matrix Composites: Processing, Modelling and Characterization,* ed. Bhagat, T., Kumar, S. and Ritter, J. E. The Minerals, Metals and Materials Society, Warrendale, PA, 1990, pp. 311–318.
29. Karandikar, P. and Chou, T. W., Characterization and modeling of microcracking and elastic moduli changes in Nicalon/CAS composites. *Composite Sci. & Technol.*, 1990, **46**(2), 253–263.
30. Evans, A. G., Domergue, J. M. and Vagaggini, E., Methodology for relating the tensile constitutive behavior of ceramic-matrix composites to constituent properties. *J. Amer. Ceram. Soc.*, 1994, **77**(6), 1425–1435.